Kinetic effects of NO addition on *n*-dodecane cool and warm diffusion flames

Mengni Zhou [a,b,*], Omar R. Yehia [a], Christopher B. Reuter [a],
Christopher M. Burger [a], Yuki Murakami [a,c], Hao Zhao [a], Yiguang Ju [a]

[a] *Department of Mechanical and Aerospace Engineering, Princeton University, NJ 08544, USA*
[b] *School of Energy and Power Engineering, Wuhan University of Technology, Wuhan, Hubei 430063, PR China*
[c] *Institute of Fluid Science, Tohoku University, 2-1-1 Katahira, Aoba, Sendai, Miyagi 980-8577, Japan*

Abstract

The kinetic effects of NO addition on the flame dynamics and burning limits of *n*-dodecane cool and warm diffusion flames are investigated experimentally and computationally using a counterflow system. The results show that NO plays different roles in cool and warm flames due to their different reaction pathway sensitivities to the flame temperature and interactions with NO. We observe that NO addition decreases the cool flame extinction limit, delays the extinction transition from warm flame to cool flame, and promotes the ignition transition from warm flame to hot flame. In addition, jet-stirred reactor (JSR) experiments of *n*-dodecane oxidation with and without NO addition are also performed to develop and validate a *n*-dodecane/NO_x kinetic model. Reaction pathway and sensitivity analyses reveal that, for cool flames, NO addition inhibits the low-temperature oxidation of *n*-dodecane and reduces the flame temperature due to the consumption of RO_2 via $NO+RO_2 \leftrightarrow NO_2+RO$, which competes with the isomerization reaction that continues the peroxy radical branching sequence. The model prediction captures well the experimental trend of the inhibiting effect of NO on the cool flame extinction limit. For warm flames, two different kinds of warm flame transitions, the warm flame extinction transition to cool flame and the warm flame reignition transition to hot flame, were observed. The results suggest that warm extinction transition to cool flame is suppressed by NO addition while the warm flame reignition transition to hot flame is promoted. The kinetic model developed captures well the experimentally observed warm flame transitions to cool flame but fails to predict the warm flame reignition to hot flame at similar experimental conditions.
© 2020 The Combustion Institute. Published by Elsevier Inc. All rights reserved.

Keywords: Diffusion flame; NO addition; Cool flame; Warm flame; Counterflow flame

* Corresponding author at: Department of Mechanical and Aerospace Engineering, Princeton University, NJ 08544, USA.

E-mail address: mengniz@princeton.edu (M. Zhou).

1. Introduction

In the challenge to adhere to more stringent restriction on carbon emissions and achieve higher engine efficiencies, various new engine technologies

such as homogenous charge compression ignition [1,2] and partially premixed compression ignition [3], aiming at low-temperature and high-pressure combustion operation, have been proposed. The autoignition and flame propagation in such systems often show a three-stage ignition and combustion process [4]. The first-stage ignition and subsequent cool flame are governed by the low-temperature peroxy branching (RO_2) chemistry. The second-stage ignition and the warm flame are governed by HO_2 chemistry at intermediate temperatures [5,6]. The third-stage ignition and the hot flame are controlled by the high-temperature small radical chemistry. To control the mixtures' ignition phasing, exhaust gas recirculation (EGR) and non-equilibrium plasma [7] are often utilized in these advanced engines. Chemically active species such as NO_x in EGR or those produced by plasma have strong kinetic effects on combustion. For example, NO can greatly alter the low- and intermediate-temperature oxidation kinetics [8–11]. However, few reports are available on the effects of NO addition on the flame dynamics and burning limits of cool and warm flames.

Since *n*-dodecane ($nC_{12}H_{26}$) is an important component of transportation fuel surrogates and has strong low-temperature chemistry [12], it is an appropriate fuel to use for the investigation of the effects of NO on cool and warm flames. However, few studies on the effects of NO on *n*-dodecane oxidation at low- and intermediate-temperatures have been performed. Moreover, although several detailed and reduced *n*-dodecane mechanisms exist in the literature [13–17], none of them contain reactions between fuel-sized molecules and NO_x. To study the kinetic effects of NO on *n*-dodecane cool and warm flames, a *n*-dodecane/NO_x model should be developed and validated.

Motivated by the above discussions, the objective of the present study is to investigate the effects of NO addition on *n*-dodecane diffusion cool and warm flames and to develop a validated skeletal *n*-dodecane/NO_x model for combustion modeling with NO addition. To accomplish this, the cool flame extinction limits and warm flame transitions, including the extinction transition to cool flame and the ignition transition to hot flames, of *n*-dodecane flames with and without NO addition are measured in a counterflow burner. Additionally, jet-stirred reactor (JSR) experiments of *n*-dodecane oxidation without and with NO addition are also performed to assist in the development of a coupled *n*-dodecane/NO_x model. A skeletal *n*-dodecane/NO_x coupling model is validated against the cool flame, warm flame, and JSR experimental data. Then, detailed kinetic analyses are performed to understand the temperature-dependent effects of NO on cool and warm flame structures and transition limits.

2. Experimental and computational methods

The kinetic experiments of *n*-dodecane oxidation with and without NO addition were performed in an atmospheric-pressure jet-stirred reactor with a spherical volume of 42 cm^3. Details of the JSR experimental setup and related uncertainties can be found in [18,19]. During the experiments, liquid *n*-dodecane (Sigma Aldrich, anhydrous, ≥99%) was injected into a heated pre-vaporizer by a syringe pump (Harvard Apparatus, PHD 22/2000), and then the vaporized *n*-dodecane gas was carried by a nitrogen stream to mix with the primary oxidizer stream (O_2/NO/Ar/N_2) in the JSR. The experimental temperatures were varied from 450 to 900 K, and the equivalence ratio was fixed at 1.3. The inlet volume flow rate was set to 969 ml/min at 295 K; hence, the residence time in the reactor varied with the temperature, ranging from 0.39–0.79 s. For species diagnostics, the reacting mixtures were sampled into a molecular beam mass spectrometry (MBMS) with sonic probes. The measurement uncertainty was around 10–20%, which was mainly induced by the species calibration for MBMS and the electron impact (20 ± 1 eV) in MBMS. The detailed experimental conditions and the temperature profile of the mixture in JSR can be seen in Table S1 and Fig. S1 of Supplemental Material. Simulations of homogeneous oxidation of *n*-dodecane were performed in the PSR [20] module of CHEMKIN package.

An atmospheric counterflow burner [21] was employed for the experiments of *n*-dodecane cool and warm diffusion flames. The main exit nozzle diameter and the separation distance of two burners are 1.3 and 2.25 cm, respectively. For the NO addition cases, NO was added to the fuel stream. The *n*-dodecane/N_2/NO gases were ejected from the upper burner with an outlet temperature of 550 ± 5 K, and the oxidizer was expelled from the bottom burner at 300 K. To generate a stable warm flame at ambient conditions, a small amount of ozone was doped into the oxidizer stream. In addition, an image intensified CCD camera (Princeton Instruments, PI-MAX4) was used to record the chemiluminescence peaks of the flames. Fig. 1 shows the chemiluminescence images of *n*-dodecane cool and warm flames. Compared to cool flame, the warm flame exhibits a two-stage flame structure (double peaks in chemiluminescence).

In the present study, the strain rates of cool flame extinction, warm flame extinction to cool flame, and warm flame reignition to hot flame were measured. The measurements were repeated three times for each condition to obtain an average strain rate. Typically, the scatter of the experimental measurements remained within ± 3 s^{-1}. Moreover, the maximum temperatures of *n*-dodecane cool and warm flames with different NO addition levels were also measured. After establishing stable cool
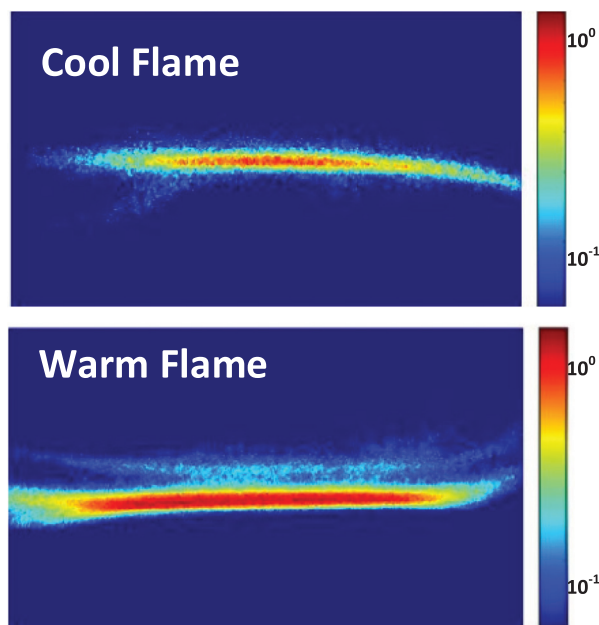
Fig. 1. Measured chemiluminescence images of *n*-dodecane cool and warm flames.

or warm flames, a thermocouple with a diameter of 0.0254 cm was slowly inserted into the flow near the upper nozzle and then was moved toward to bottom nozzle to determine the maximum flame temperatures, which have approximately ± 10 K uncertainty. Numerical computations of *n*-dodecane diffusion flame extinction limits were performed using the OPPDIF [22] module of the CHEMIN package. Extinction-to-ignition S-curves (Figs. 4 and 8) were generated by a modified arc-length continuation method [23].

3. Results and discussion

3.1. Chemical mechanism selection and validation

In order to obtain a skeletal *n*-dodecane/NO$_x$ kinetic model that can reasonably and computationally efficiently predict *n*-dodecane cool and warm diffusion flames without and with NO addition, the following procedures were performed. First, based on the measured cool flame extinction (CFE) limits for pure *n*-dodecane, two *n*-dodecane kinetic models were selected from a variety of reduced models. Second, the JSR experiments of *n*-dodecane oxidation with NO addition were performed to validate *n*-dodecane/NO$_x$ coupling reactions and NO$_x$ sub-mechanisms. Two *n*-dodecane/NO$_x$ reduced models were then generated by coupling the two selected *n*-dodecane reduced mechanisms with the validated *n*-dodecane/NO$_x$ coupling reactions and NO$_x$ sub-

mechanisms. The *n*-dodecane/NO$_x$ model with a better predictability of *n*-dodecane oxidation in JSR and cool flames was used in the present study.

Fig. 2 shows the comparison between the experimental measurements and several model predictions for the CFE limits of pure *n*-dodecane. In these models, the Cai model [13] and the LLNL_R model [14], based upon their detailed model, are reduced to 141 and 145 species, respectively, using the path flux analysis method [24]. The other reduced models are chosen directly from the literature [15–17]. As shown in Fig. 2, the reduced Cai and Yao models show a better prediction for the neat *n*-dodecane CFE limits and are hence chosen as the candidate models.

To develop the *n*-dodecane/NO$_x$ coupling reactions and NO$_x$ sub-mechanisms, jet-stirred reactor experiments of *n*-dodecane oxidation between 450 and 900 K at an equivalence ratio of 1.3 without and with 300 ppm NO addition are performed. For reactions between fuel-sized molecules and NO, the *n*-dodecane/NO$_x$ coupling reactions are taken as analogies to Anderlohr [25] (i.e., R+NO$_2$↔RO+NO, RO$_2$+NO↔RO+NO$_2$, etc.). For the basic nitrogen chemistry, the NO$_x$ sub-mechanism is selected from HP-Mech [26]. To reduce the uncertainties of *n*-dodecane mechanism itself, the detailed LLNL *n*-alkane [14] mechanism is used to generate a LLNL/NO$_x$ model as an initial test.

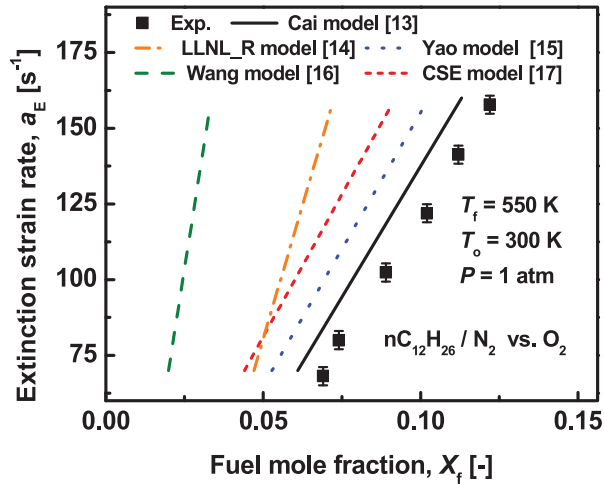The measured and computed mole fraction profiles of *n*-dodecane with and without NO addition

Fig. 2. Comparison between the different models on the prediction of the extinction limits for *n*-dodecane diffusion cool flames.
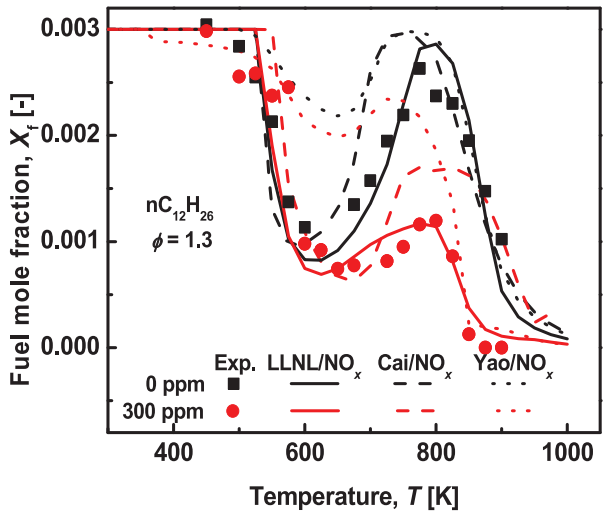

Fig. 3. Predicted and measured temperature evolutions of the mole fraction of *n*-dodecane at fuel rich condition without and with 300 ppm NO addition in JSR.

in JSR are shown in Fig. 3. It is clear that NO has a significant effect on *n*-dodecane oxidation, inhibiting the low-temperature oxidation at temperatures below 625 K. However, it weakens the NTC effect and accelerates intermediate-temperature fuel oxidation above 775 K. The LLNL/NO$_x$ model shows a good prediction of *n*-dodecane oxidation both with and without NO addition, indicting reasonable accuracy of the current *n*-dodecane/NO$_x$ coupling reactions and NO$_x$ sub-mechanisms.

It is known that the low-temperature kinetics in detailed models is very sensitive to exothermic reactions of fuel radicals and isomers and that reliable prediction of isothermal reactor experiments is no

guarantee of reliable prediction of flame behavior due to thermal chemical coupling [12]. Therefore, even though the detailed LLNL/NO$_x$ mechanism predicts *n*-dodecane JSR oxidation well at present experimental conditions, the reduced LLNL model is not considered due to its poor prediction of the CFE limit of *n*-dodecane flames (Fig. 2).

Based on the above, the Yao/NO$_x$ and reduced Cai/NO$_x$ models were assembled. Comparing the fuel mole fractions between the simulated results by these two models and the experimental data in the JSR, it is seen that the Yao/NO$_x$ model captures the high-temperature oxidation of *n*-dodecane, whereas Cai/NO$_x$ performs
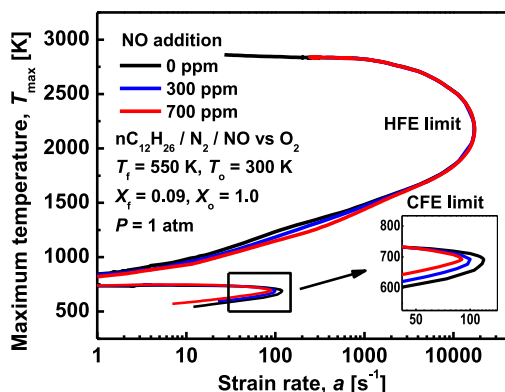
Fig. 4. Calculated S-curves of *n*-dodecane diffusion flames with different NO addition levels.

better at low and intermediate temperatures. Therefore, although the Cai/NO$_x$ model cannot quantitatively predict *n*-dodecane oxidation at temperatures above 725 K, the trends of the effect of NO addition on *n*-dodecane oxidation are better captured than the Yao/NO$_x$ model. The reduced Cai/NO$_x$ model is therefore employed for the remainder of this study and is available in the Supplementary Material.

3.2. Effects of NO addition on the near-limit behavior of n-dodecane hot and cool diffusion flames

Fig. 4 presents calculated S-curves of *n*-dodecane diffusion flames in the counterflow geometry at 9% mole fraction of *n*-dodecane ($X_f = 0.09$),

pure oxygen ($X_o = 1$), and 1 atm with different NO addition levels. In all cases, two stable flame branches, a hot flame above 2100 K (HF) and a cool flame around 700–750 K (CF), and two stretch extinction limits, hot flame extinction (HFE) limit and cool flame extinction (CFE) limit, can be seen. The numerical calculations also show the effect of NO addition on the *n*-dodecane hot diffusion flame is negligible at this condition. This is expected because the hot flame is governed by the fast, high-temperature chain-branching reaction H + O$_2$ ↔ O + OH, which is minimally affected by the small amounts of NO addition at this condition. However, the differences in the cool flames among three different NO addition cases can be observed. The CFE limit is reduced from 119 s^{-1} to 90 s^{-1} with 700 ppm NO addition, indicating that NO inhibits the low-temperature chemistry of *n*-dodecane cool flames.

To further confirm the effects of NO addition on *n*-dodecane cool flame, the CFE limits of *n*-dodecane with different levels of NO addition are experimentally determined, as shown in Fig. 5. It is seen that the extinction strain rates increase with the fuel mole fraction and decrease with NO addition. Moreover, the inhibition effect of NO on the CFE limits becomes more evident at a high fuel concentration. The current model can reasonably capture the general trend of the experiments and show a good prediction for both pure *n*-dodecane and NO addition cases at low fuel concentrations. However, it over-predicts the CFE limits for NO addition cases at high fuel concentration.

To elucidate the kinetic effects of NO on *n*-dodecane cool diffusion flames, the cool flame structures for pure *n*-dodecane with and without 700 ppm NO addition cases are shown in Fig. 6, and the rate of production analyses of major
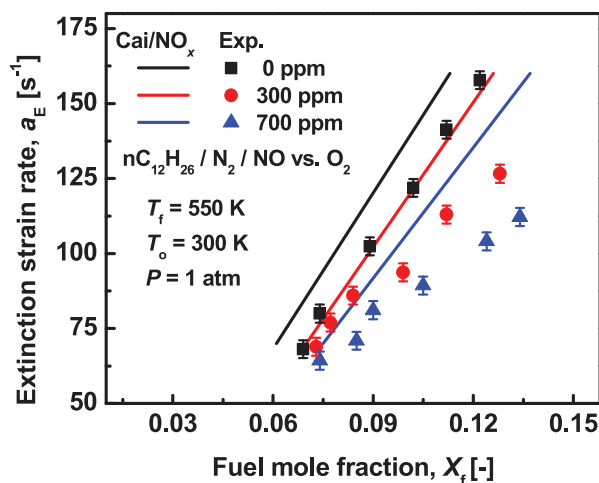

Fig. 5. Comparison between the measured and computed extinction limits of *n*-dodecane cool diffusion flames as a function of the fuel mole fraction with three different levels of NO addition.
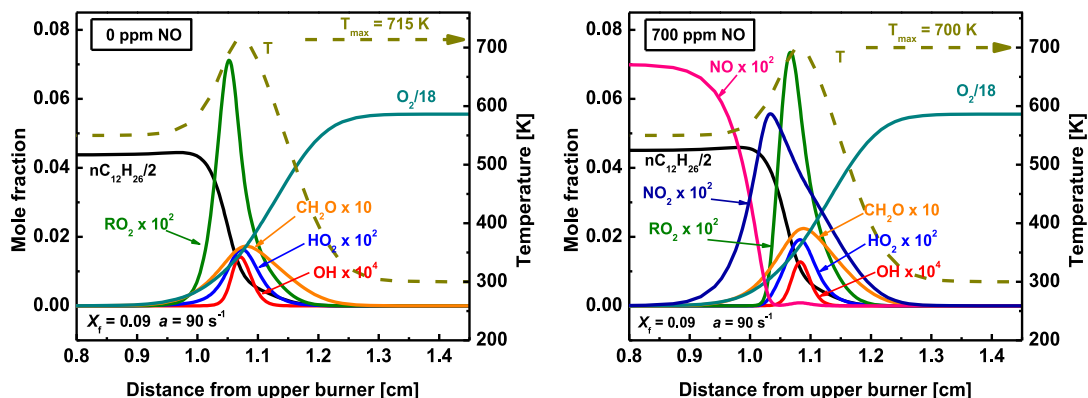
Fig. 6. Calculated flame structures of *n*-dodecane cool diffusion flames without (left) and with 700 ppm (right) NO addition at $X_f = 0.09$ and $a = 90 \ s^{-1}$. The fuel nozzle is located at $x = 0$ cm.
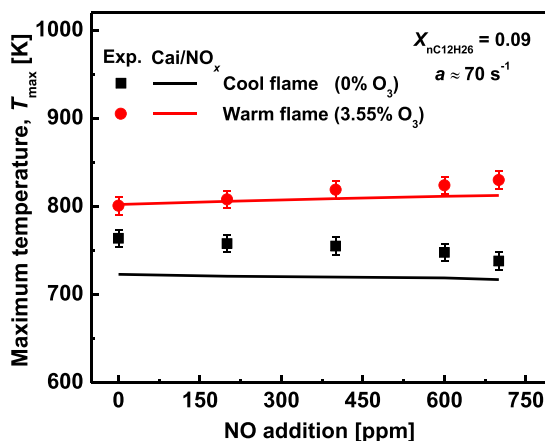

Fig. 7. Measured maximum temperatures of *n*-dodecane flame with various NO additions.

species are also performed. It is seen that the flame temperature decreases with NO addition. This decreasing trend is also confirmed by the experimentally measured maximum temperatures of *n*-dodecane cool flames with increasing concentrations of NO addition (Fig. 7).

From the flame structures and NO consumption path flux, it is noted that NO is quickly consumed via $RO_2 + NO \leftrightarrow RO + NO_2$ (75%) and $NO + HO_2 \leftrightarrow OH + NO_2$ (25%). A temperature sensitivity analysis has been performed and is shown in Fig. S2 of Supplemental Material. The $RO_2 + NO \leftrightarrow RO + NO_2$ reaction has a negative sensitivity, indicating that this reaction decreases the cool flame temperature. On the other hand, $NO + HO_2 \leftrightarrow OH + NO_2$ has a positive sensitivity to flame temperature. Note that the cool flame is governed by low-temperature reactivity and the major chain-branching reaction pathway is $RO_2 \rightarrow QOOH \rightarrow O_2QOOH \rightarrow OQ'O + 2OH$. Since NO consumes RO_2, this slows down the chain-branching process. Hence, although some NO reacts with HO_2 to produce OH radicals and enhance the reactivity, the negative effect of $RO_2 + NO \leftrightarrow RO + NO_2$ on chain-branching is much stronger, leading to the decrease of cool flame temperature.

Moreover, Fig. 6 also shows that the rapid consumption of NO leads to a high concentration of NO_2. In the reaction zone, $NO_2 + CH_3 \leftrightarrow NO + CH_3O$ is therefore promoted to accelerate the endothermic reaction $CH_3O + O_2 \leftrightarrow CH_2O + HO_2$ and further reduce the cool flame temperature. This process can also be seen directly from the increasing mole fractions of HO_2 and CH_2O with NO addition. In addition, the small local peak in the NO mole fraction profile shows that the inter-conversion reactions between NO and NO_2 [19] extends the impact of NO on *n*-dodecane cool diffusion flames.
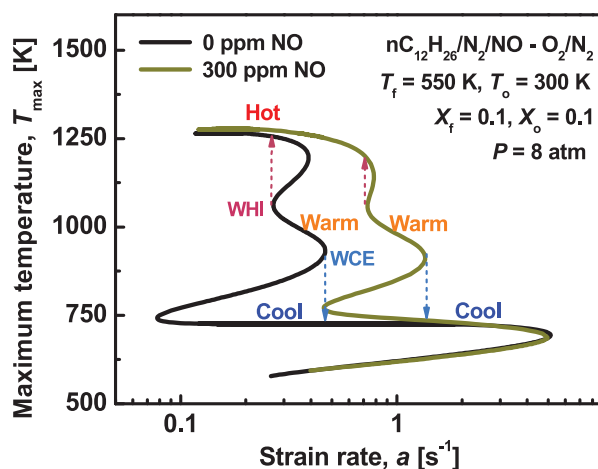
Fig. 8. Calculated S-curves depicting different flame regimes with and without NO additions.

3.3. Effects of NO on n-dodecane warm diffusion flame burning limits and transitions

The above discussed the impacts of NO addition on *n*-dodecane hot and cool flames. However, a multistage warm diffusion flame can exist between the cool and the hot flames [6,27]. As previously discussed [27], the warm flame plays a critical role in the transition from cool flame to hot flame. To demonstrate the effect of NO on the dynamics of the warm flame, the strain rates of extinction transitions from warm flames to cool flames and ignition transitions from warm flames to hot flames of *n*-dodecane diffusion flames with and without NO addition are computed and measured. The warm flame exhibits a two-staged flame structure, as the experimental images show in Fig. 1. Here, the warm flame is defined as a flame with double chemiluminescence peaks in the experiments and with double heat release peaks in the computations.

Since a stable warm flame cannot be computationally established at 1 atm without ozone, as shown in Fig 4, the boundary conditions of $X_o = 0.1$, $X_f = 0.1$ and 8 atm are used to illustrate the dynamics of warm flames in Fig. 8. It is clearly seen that a warm flame can extinguish to a cool flame from the extinction transition point (WCE) with the temperature decreasing or can jump to the hot flame though the ignition transition point (WHI) with the increase of temperature. Moreover, the strain rates of both WCE and WHI increase with NO addition, indicating that NO delays the warm flame extinction to cool flame and promotes the transition to hot flame.

The measured strain rates of WCE and WHI of *n*-dodecane flames assisted by a small percentage of ozone at 1 atm without and with 700 ppm NO addition are shown in Fig. 9. It is seen that, similar to the computation results, the warm flames

extinguish to cool flames and the warm flames ignite to hot flames at higher strain rates with NO addition. The model captures well the behavior of WCE; however, numerical solutions failed to show a distinct WHI. Since WHI is very sensitive to the kinetic model, future improvement of the model predictability of WHI is needed.

To elucidate the effect of the NO addition on the warm flame structures, the reaction heat release profiles and flame structures at $X_f = 0.06$ and $a = 120$ s^{-1} with and without NO addition are presented in Figs. 10 and 11, respectively. It is important to note that the warm flame exhibits a two-stage flame structure: the first-stage oxidation is governed by peroxy branching low-temperature chemistry related to the parent fuel and the second-stage oxidation is dominated by the intermediate-temperature combustion of intermediate products from the first-stage oxidation. From the heat release distribution, it is noted that the heat release of the typical reactions in low-temperature chemistry, such as $R + O_2 \leftrightarrow RO_2$, are reduced with NO addition, while the heat release of the reactions which are favored at intermediate temperatures, e.g., $C_2H_3 + O_2 \leftrightarrow CH_2O + HCO$, are increased. Hence, the total heat release in the first and second oxidation stage decreases and increases, respectively. This indicates that NO inhibits the first-stage oxidation and promotes the second-stage oxidation in the warm flame. Therefore, NO addition delays the warm-cool flame transitions.

From the warm flame structures in Fig. 11, the flame temperature rises by 15 K with NO addition, as confirmed by experimental measurements (Fig. 7). NO is rapidly consumed by RO_2 to generate NO_2. Moreover, the concentration of RO_2 decreases, and the concentrations of OH and HO_2 increase with NO addition. Again, the NO consumption path flux is
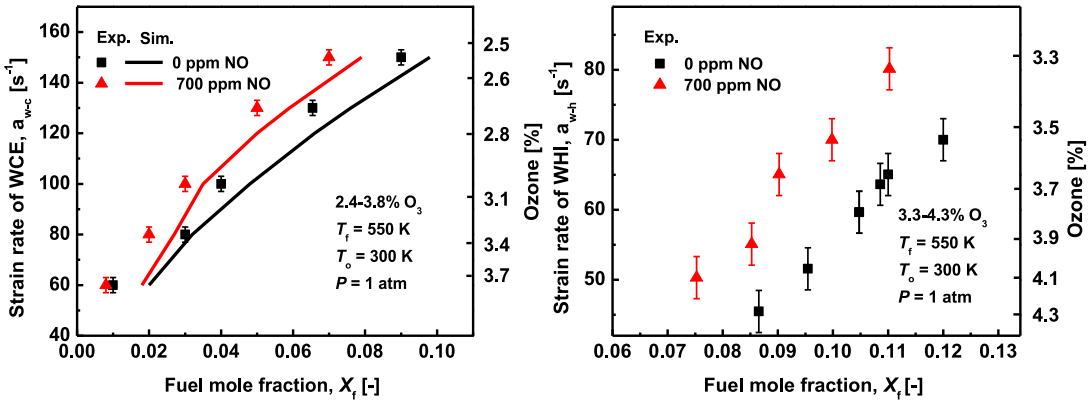
Fig. 9. Measured and computed the strain rates of WCE (left) and WHI (right) of *n*-dodecane flames without and with 700 ppm NO addition. .
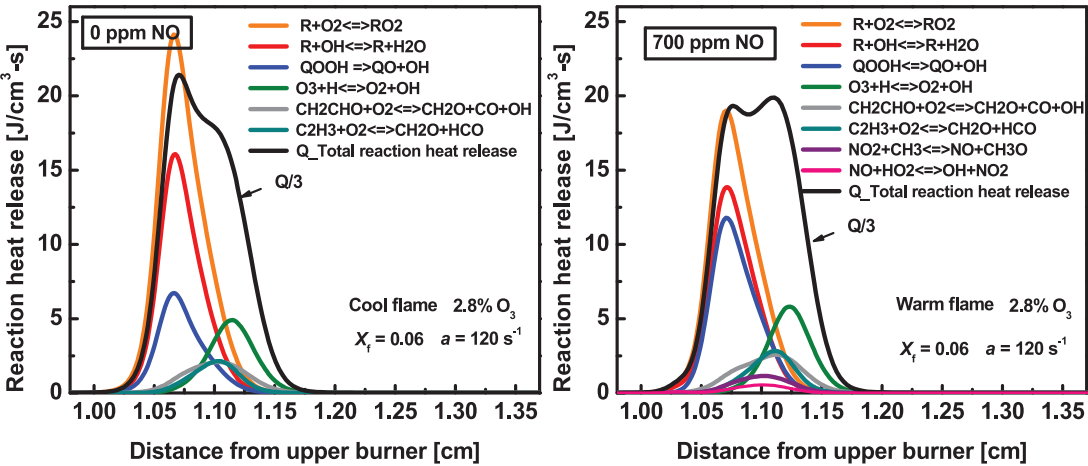

Fig. 10. Calculated major reactions heat release for *n*-dodecane diffusion flames at without and with NO addition at $X_f = 0.06$ and $a = 120 \text{ s}^{-1}$. The fuel nozzle is located at $x = 0$ cm.
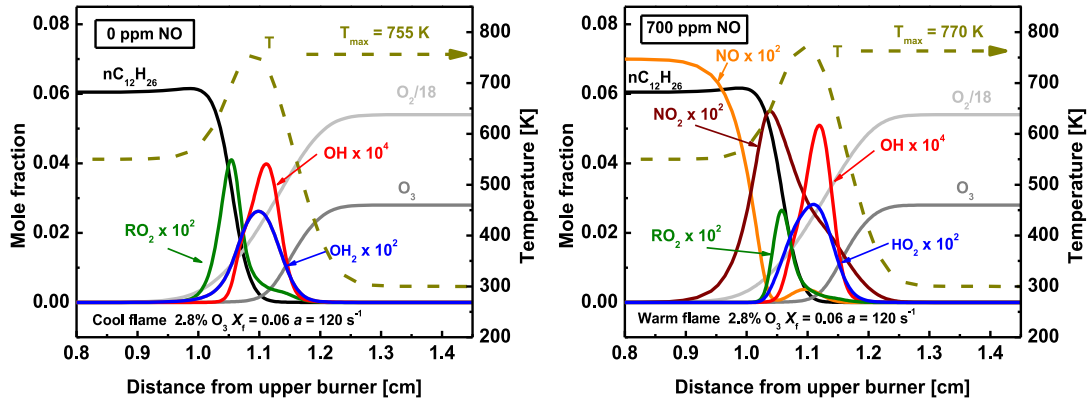

Fig. 11. Calculated flame structures of *n*-dodecane diffusion flames without (a) and with 700 ppm (b) NO addition at $X_f = 0.06$ and $a = 120 \text{ s}^{-1}$. The fuel nozzle is located at $x = 0$ cm.

obtained showing $NO+HO_2\leftrightarrow OH+NO_2$ (59%) and $RO_2+NO\leftrightarrow RO+NO_2$ (31%). Based on the above information, the kinetic effect of NO on the warm flame can be concluded as follows. NO inhibits the first-stage cool flame oxidation via $NO+RO_2\leftrightarrow RO+NO_2$. Since the concentration of RO_2 at this temperature is relatively low, the inhibition effect of NO on the first-stage oxidation does not result in the increased tendency of cool flame to extinguish. Instead, the reaction $NO+HO_2\leftrightarrow OH+NO_2$ converts the less reactive HO_2 to more reactive OH radicals and enhances the intermediate-temperature chemistry of the warm flame. Moreover, due to the increasing warm flame temperature, the reaction $QOOH\rightarrow QO+OH$ is also accelerated for radical production. Therefore, the second-stage oxidation in the warm flame is promoted with NO addition. Additionally, the favorable effect of NO at intermediate temperature accelerates the warm flame reignition to a hot flame.

4. Conclusions

The effect of NO on the dynamics and burning limits of *n*-dodecane cool and warm diffusion flames were investigated experimentally and numerically using the counterflow flame configuration. A skeletal *n*-dodecane/NO_x kinetic model was assembled and validated via jet-stirred reactor species profiles and cool flame extinction limits of *n*-dodecane mixtures with and without NO addition.

The ignition and extinction S-curves of *n*-dodecane diffusion cool flames, warm flames, and hot flames with different NO addition levels were obtained. It is found that NO addition significantly inhibits the cool flame extinction limits. Kinetic analysis shows that NO suppresses low-temperature oxidation via $NO+RO_2\leftrightarrow NO_2+RO$ and decreases the flame temperature and fuel reactivity in the cool flame. The model prediction is in qualitative agreement with the experimentally measured inhibiting effect of NO on the cool flame extinction limit.

Two different types of warm flame transitions, warm flame extinction transition to cool flame and the warm flame reignition transition to hot flame, of *n*-dodecane with and without NO addition were observed. The results showed that warm flame extinction transition to cool flame was delayed by NO addition while the warm flame reignition transition to hot flame was promoted. The kinetic model captured well the experimentally observed warm flame transitions to cool flame and hot flame but failed in predicting the warm flame reignition transition to hot flame at similar experimental conditions. Kinetic analysis of warm flame structures shows that NO addition inhibits the first-stage cool flame chemistry but promotes the second-stage fuel oxidation governed by intermediate-temperature chemistry via the $NO+HO_2\leftrightarrow NO_2+OH$ and $QOOH\rightarrow OH+QO$ reactions. Future work is needed to improve the *n*-dodecane/NO_x model to capture the warm flame reignition transition to hot flame.

Declaration of Competing Interest

None.

Supplementary materials

Supplementary material associated with this article can be found, in the online version, at doi:10.1016/j.proci.2020.06.002.

References

[1] J.E. Dec, *Proc. Combust. Inst.* 32 II (2009) 2727–2742.
[2] X. Lu, D. Han, Z. Huang, Prog. Energy Combust. Sci. 37 (20).
[3] M.P.B. Musculus, P.C. Miles, L.M. Pickett, *Prog. Energy Combust. Sci.* 39 (2013) 246–283.
[4] Y. Ju, C.B. Reuter, O.R. Yehia, T.I. Farouk, S.H. Won, *Prog. Energy Combust. Sci.* 75 (2019) 100787.
[5] T. Zhang, Y. Ju, *Combust. Flame.* 211 (2020) 8–17.
[6] O.R. Yehia, C.B. Reuter, Y. Ju, *Combust. Flame.* 195 (2018) 63–74.
[7] Y. Ju, W. Sun, *Prog. Energy Combust. Sci.* 48 (2015) 21–83.
[8] M. Amann, T. Alger, D. Mehta, *SAE Int. J. Engines.* 4 (2011) 235–245.
[9] G. Moréac, P. Dagaut, J.F. Roesler, M. Cathonnet, *Combust. Flame.* 145 (2006) 512–520.
[10] L. Marrodán, Y. Song, O. Herbinet, M.U. Alzueta, C. Fittschen, Y. Ju, F. Battin-Leclerc, *Chem. Phys. Lett.* (2019) 22–26.
[11] T. Amano, F.L. Dryer, *Symp. Combust.* (1998) 397–404.
[12] C.B. Reuter, M. Lee, S.H. Won, Y. Ju, *Combust. Flame.* 179 (2017) 23–32.
[13] L. Cai, H. Pitsch, S.Y. Mohamed, V. Raman, J. Bugler, H. Curran, S.M. Sarathy, *Combust. Flame* 173 (2016) 468–482.
[14] C.K. Westbrook, W.J. Pitz, O. Herbinet, E.J. Silke, H.J. Curran, *States Sect. Inst. Fall Meet.* (2007) 130–196 Western States Section/Combustion Institute, 2007.
[15] T. Yao, Y. Pei, B.J. Zhong, S. Som, T. Lu, K.H. Luo, *Fuel* 191 (2017) 339–349.
[16] H. Wang, Y. Ra, M. Jia, R.D. Reitz, *Fuel* 136 (2014) 25–36.

[17] C.C. Fuller, P. Gokulakrishnan, M.S. Klassen, S. Adusumilli, Y. Kochar, D. Bloomer, J. Seitzman, H.H. Kim, S.H. Won, F.L. Dryer, Y. Ju, B.V. Kiel, *50th AIAA Aerosp. Sci. Meet. Incl. New Horizons Forum Aerosp. Expo.* (2012).

[18] H. Zhao, L. Wu, C. Patrick, Z. Zhang, Y. Rezgui, X. Yang, G. Wysocki, Y. Ju, *Combust. Flame* 197 (2018) 78–87.

[19] H. Zhao, A.G. Dana, Z. Zhang, W.H. Green, Y. Ju, *Energy* (2018) 727–738.

[20] Glarborg P., Kee R J., Grcar J F., et al. . Sandia Report SAND86-8209, 1986.

[21] C.B. Reuter, R. Zhang, O.R. Yehia, Y. Rezgui, Y. Ju, *Combust. Flame* 196 (2018) 1–10.

[22] A. Lutz, R. Kee, J. Grcar, F. Rupley, *Sandia Natl. Lab.* (1997) 3–33.

[23] Y. Ju, H. Guo, K. Maruta, F. Liu, *J. Fluid Mech* 342 (1997) 315–334.

[24] W. Sun, Z. Chen, X. Gou, Y. Ju, *Combust. Flame* 157 (2010) 1298–1307.

[25] J.M. Anderlohr, R. Bounaceur, A. Pires Da Cruz, F. Battin-Leclerc, *Combust. Flame* 156 (2009) 505–521.

[26] http://engine.princeton.edu/mechanism/HP-Mech.html

[27] E. Lin, C.B. Reuter, Y. Ju, *Proc. Combust. Inst.* 37 (2019) 1791–1798.